Available online at www.sciencedirect.com

ScienceDirect

Scripta Materialia 106 (2015) 42–45

Scripta MATERIALIA

www.elsevier.com/locate/scriptamat

Thermally activated deformation processes in body-centered cubic Cr – How microstructure influences strain-rate sensitivity

Verena Maier,* Anton Hohenwarter, Reinhard Pippan and Daniel Kiener

Montanuniversität Leoben, Department Materials Physics & Erich-Schmid-Institute for Materials Sciences, Austrian Academy of Science, Jahnstr. 12, A-8700 Leoben, Austria

Received 31 March 2015; revised 29 April 2015; accepted 1 May 2015
Available online 26 May 2015

The microstructure dependent deformation behavior of chromium, especially in terms of strain-rate sensitivity (SRS), was studied by means of improved nanoindentation methods as a function of temperature. Cr was investigated in the single crystalline (sx) and ultrafine-grained (ufg) condition. With increasing temperature a decreasing SRS was determined for sx-Cr, while for ufg-Cr a significant increase upon overcoming the critical temperature T_c was measured. This is attributed to the increased importance of dislocation–grain boundary interactions, and a change in the dominating deformation behavior.

Keywords: High temperature nanoindentation; Critical temperature; bcc; ufg

Over the last decades, the underlying deformation mechanisms in body-centered cubic (bcc) metals were of great interest [1–6]. Generally, the deformation of single crystalline (sx) bcc metals significantly differs from that of face-centered cubic (fcc) metals [5,6]. Below a critical temperature T_c, the deformation resistance of bcc metals becomes strain-rate sensitive, as the motion of screw dislocations via the kink pair mechanism requires a thermally activated stress component σ^*. This thermal stress component mainly consists of the high Peierls potential in bcc metals, related to a complicated three-dimensional core structure of $a_0\langle 1\,1\,1\rangle/2$ screws dislocation [7,8]. With increasing testing temperature up to a material specific critical temperature T_c, the thermal stress component σ^* decreases, while the potential athermal stress component σ_a is comparatively high and thus dominates the mechanical behavior. Contrarily, for fcc metals the Peierls potential requires no additional thermal activation of dislocation mobility and these materials are conventionally not strain-rate sensitive below T_c. However, by refining the grain size, thermally activated processes become dominant in fcc as well, resulting in a strain-rate sensitivity SRS [6].

A recent comparison of sx-W and ufg-W demonstrated that for the fine-grained microstructure a reduction of the SRS is measured [9]. However, this was related to the higher hardness of the ultrafine-grained (ufg) material due to Hall–Petch strengthening, since the resultant strain-rate dependent hardness difference was identical for the ufg- and sx-states, respectively. Thus, it was concluded that the increase in athermal stress component due to grain refinement does not diminish the thermally activated component σ^*, but shifts the Peierls component to higher stress levels.

Up to now, only few studies investigated the direct temperature dependent deformation behavior of bcc-metals on a macroscopic [3–6,10] or local scale [1–2,9,11], with particular focus on SRS, by changing the homologous testing temperature.

In this study, the microstructure dependent small-scale deformation behavior of chromium, especially in terms of SRS, was studied by means of advanced nanoindentation strain-rate jump testing methods [12] at room and elevated temperatures exceeding T_c. In fact, Cr with a $T_c \sim 180$ °C [13–16] was studied up to 300 °C regarding influences of testing temperature and grain refinement affecting the dominating deformation behavior.

Sx-Cr was purchased from Mateck in (1 0 0) orientation, and ufg-Cr (Ducropur) was produced by means of high-pressure torsion (HPT). Therefore, disks with a diameter of 26 mm and a thickness of ~9 mm were subjected to HPT at a pressure of ~5.4 GPa to 10 revolutions at room temperature [17]. Cross-sections of all samples (sx-Cr and ufg-Cr) were prepared for metallographic examinations and nanoindentation testing. The specimens were mechanically ground, subsequently polished with diamond suspension down to 1 μm, and finally electrolytically polished to remove any remaining deformation layer.

For the ufg-state, the grain structure was analyzed using the back-scattered electron detector in a scanning electron

* Corresponding author.

http://dx.doi.org/10.1016/j.scriptamat.2015.05.001
1359-6462/

microscope (SEM/FIB, Crossbeam 1540 EsB, Zeiss, Oberkochen, Germany). The median grain size of the ufg-material was evaluated using the line intersection method on SEM images, where no distinction between high or low angle boundaries was made, as ~0.3 μm.

Nanoindentation experiments were conducted using a Nanoindenter G200 (Agilent Technologies, Chandler, AZ, USA now Keysight Technologies) equipped with a continuous stiffness measurement (CSM) unit and a three-sided diamond Berkovich pyramid (Synton, Switzerland). Machine stiffness and tip shape calibrations were performed according to the Oliver–Pharr method [18] and nanoindentation testing was carried out at room temperature (22 °C) and elevated temperatures (100 °C, 300 °C), respectively. Elevated testing temperatures were realized with a Laser Heating Stage (SurfaceTec, Hückelhoven, Germany), where tip (Sapphire–Berkovich) and sample are independently heated to adjust and stabilize the contact temperature, minimize thermal drift influences, and guarantee a well defined homogeneous temperature distribution during indentation. The thermal drift for all testing temperatures was minimized to less than 0.1 nm/s and determined previously to each indentation array.

The local SRS was measured using nanoindentation strain-rate jump tests after Maier et al. [12]. For studying the influence of microstructure and temperature, reversible strain-rate jump tests from 0.025 s^{-1} to 0.005 s^{-1}, or 0.0025 s^{-1}, respectively, were performed at 500 nm and 1500 nm, and back to the initial strain-rate at 1000 nm and 2000 nm indentation depth, respectively. The chosen strain-rates are equivalent to indentation strain-rates of 0.05 s^{-1}, 0.01 s^{-1} and 0.005 s^{-1} ($\dot{h}/h = \frac{1}{2}\dot{P}/P$). Furthermore, standard constant strain-rate (cSR) experiments (0.025 s^{-1}) were carried out up to 2500 nm indentation depth. For all strain-rate controlled tests, the CSM frequency was set to 45 Hz and a harmonic amplitude of 2 nm was superimposed. At room temperature six and at elevated temperatures four indentations, respectively, were performed for each indentation method, temperature, and microstructure.

To quantify strain-rate dependent changes in hardness, the local SRS m can be determined as $m = \partial \ln H / \partial \ln \dot{\varepsilon}$. Due to the depth dependent hardness of the sx-Cr, the SRS parameter m was directly evaluated at each indentation jump depth, which allows a determination unaffected by a possible indentation size effect, see also [9].

Figure 1 shows a QBSD image of the investigated ufg-Cr microstructure with grain sizes of ~300 nm. The grains have an equiaxed shape and are equally distributed in size and orientation.

The depth dependent hardness for sx-Cr in comparison with ufg-Cr is shown in Figure 1b. By refining the grain structure, the hardness increases due to Hall–Petch-hardening. To quantify the grain refining influence and take the indentation size effect (ISE) into account, the macroscopic hardness H_0 was evaluated from this data according to Nix–Gao. The analysis led to macroscopic hardness values of $H_{0\text{-ufg}} = 4.5$ GPa and $H_{0\text{-sx}} = 1.6$ GPa, respectively, in accordance with [19–21].

The microstructure and temperature dependent mechanical properties (load–displacement-curves, hardness, and Young's Modulus) for sx-Cr (Fig. 2a) and ufg-Cr (Fig. 2b) are investigated using nanoindentation strain-rate jump testing. Corresponding SEM images of exemplary indentations are displayed in the Supplementary Figure S.1. Tests

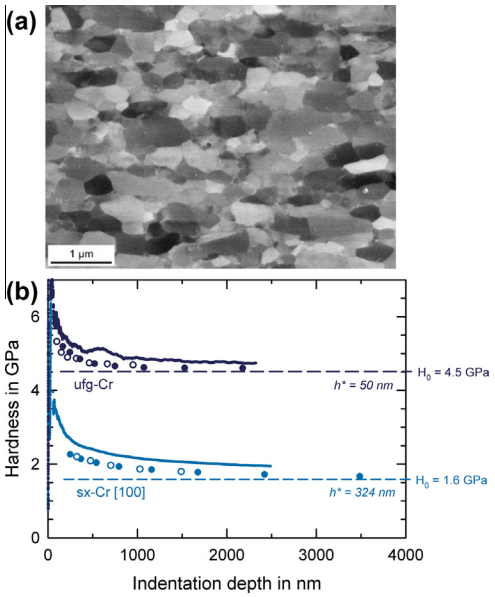

Figure 1. (a) Microstructure of ufg-Cr, as resolved by SEM, and (b) corresponding hardness of the ufg-state (upper data – dark blue) compared to the sx-state (lower data – light blue) (cSR and constant load-rate data sets). (For interpretation of the references to color in this figure legend, the reader is referred to the web version of this article.)

were performed at RT, 100 °C, and 300 °C to ensure testing underneath and above T_c, which is reported in the literature between 140 °C and 200 °C, dependent on strain-rate, impurity content, strain-path, and microstructure [13–16].

With increasing temperature, the load to reach 2500 nm indentation depth decreases from 300 mN at RT to 120 mN at 300 °C for sx-Cr, and from 600 mN at RT to 400 mN at 300 °C for ufg-Cr, respectively. The corresponding elastic modulus of ~290 GPa is strain-rate and depth independent for all states and temperatures as expected, showing just a slight decrease with T, in accordance with the literature [22]. For sx-Cr it is observed that the hardness decreases significantly with increasing temperature. More importantly, it is strongly affected by changes in strain-rate and temperature. With increasing T the influence of strain-rate changes is less pronounced for 100 °C, almost negligible for 300 °C. For the ufg-Cr the hardness behaves differently; while at RT the hardness is depth independent and little influenced by strain-rate jumps, with increasing temperature the ISE affected behavior increases and the hardness jumps get more pronounced.

For the corresponding indentations (see Supplementary Fig. S.1), no significant influence of the changing temperature is noticed. The surface appears oxidation free and the shape of the imprints is almost unchanged. Most importantly, no changes in the grain size were detected for the ufg-Cr.

Quantitatively evaluated, the SRS in Cr reduces with decreasing grain size at RT from 0.07 (sx-Cr) to 0.02 (ufg-Cr), see Figure 3a, while the hardness strongly increases due to Hall–Petch-hardening (see also Fig. 1). For increasing T the results are also presented in Figure 3a. While for ufg-Cr underneath T_c almost no change in SRS is apparent, exceeding T_c leads to an increase of m to 0.03. For sx-Cr the behavior differs significantly, with increasing T the calculated SRS decreases

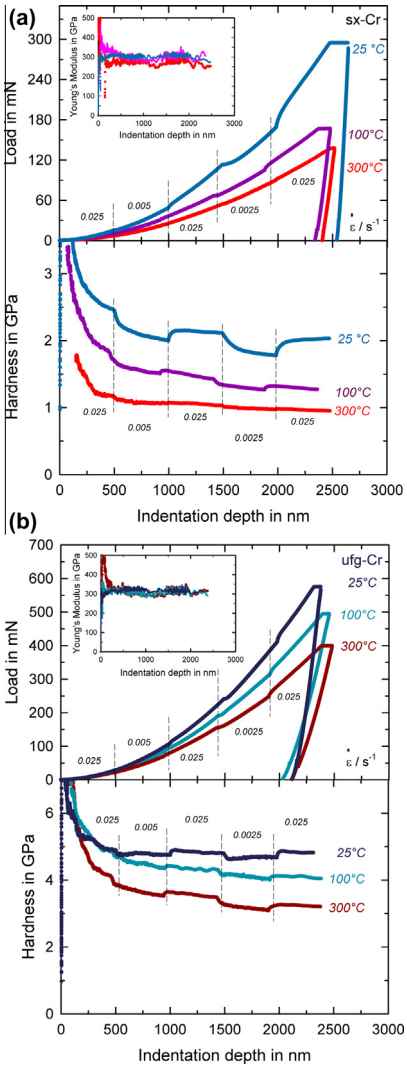

Figure 2. Nanoindentation strain-rate jump tests at room temperature, 100 °C, and 300 °C; (a) sx-Cr – load–displacement-data, modulus (inset), and hardness, (b) ufg-Cr – load–displacement-data, modulus (inset), and hardness.

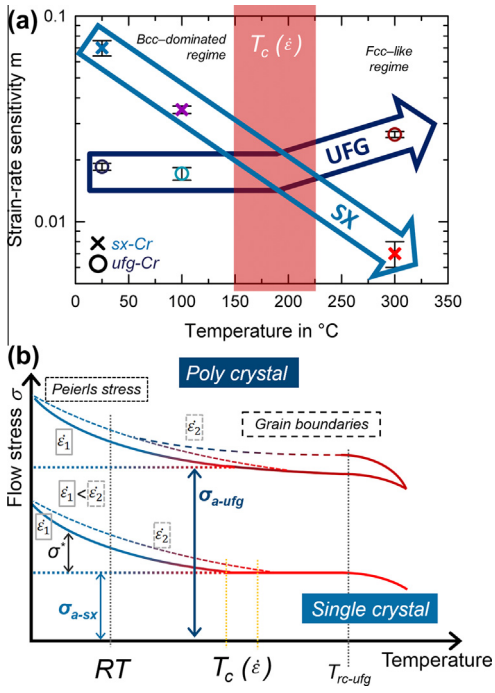

Figure 3. (a) Temperature dependent SRS m of sx-Cr and ufg-Cr below and above T_c, respectively, and (b) schematic depicting the deformation behavior of bcc-metals showing the interplay between microstructure and temperature. See text for explanatory details.

linearly to a value of about 0.001 at 300 °C, which is well in the range known for coarse grained fcc metals, indicating a strain-rate insensitive deformation behavior not limited by thermally activated processes.

To understand the underlying deformation mechanism in bcc Cr better, the temperature-dependent SRS of sx- and ufg-Cr was analyzed in detail. Figure 3b presents a schematic diagram, explaining the interplay of different contributions to the flow stress, starting with the established components and extending those for non-ambient conditions and refined microstructures. For sx and coarse grained bcc-samples, the thermally activated stress component σ^*, and thus the motion of screw dislocations, dominates the macroscopic as well as the local deformation behavior underneath T_c [1,8,11]. During severe plastic deformation, forest dislocations and a high density of grain boundaries are formed. From recent studies on nanocrystalline bcc-metals with grain sizes smaller 300 nm, it is known that the deformation is mainly governed by edge dislocations [23–24], and the thermally activated contribution of screw dislocations is completely omitted for grain sizes below 100 nm. This might further affect the time dependent deformation behavior. However, a complete disappearance of SRS cannot be explained since from fcc metals it is known that the interaction of edge dislocations and grain boundaries leads again to a thermally activated component of the flow stress [6]. For grain sizes between 100 nm and 1 μm, as in the present work, the material specific Peierls-barrier stays thereby the same in the ufg- and cg-state [9]. The athermal component of the flow stress of the ufg-material, $\sigma_{a\text{–ufg}}$, however, increases with decreasing grain size due to the dominant Hall–Petch strengthening. Here, an increase in equivalent indentation stress σ_a ($\sigma = H/C^*$; for a Berkovich tip at a representative strain of 8% and a constraint factor $C^* = 2.8$) of 0.95 GPa was evaluated based on the macroscopic hardness H_0 of sx-Cr and ufg-Cr, respectively.

Regarding the SRS (Fig. 3a), the high athermal stress component in ufg-Cr directly leads to a reduced contribution of the thermally activated component σ^* to the overall strength of the ufg-material. This is reflected by a non-negligible SRS for the ufg sample, which is, however, significantly reduced compared to that of the sx-specimen. This can be also seen in the depth-dependent hardness (Fig. 2), where a change in the applied strain-rate by an order of magnitude directly leads to a change in hardness of about 0.3 GPa for sx-Cr and only 0.15 GPa for the ufg-state. For the ufg-states, the high number of grain-boundaries, the dislocation motion, governed by both the kink pair nucleation and climbing of edge dislocations, as well as the dislocation annihilation near these boundaries might play an additional role. This leads to an overall further contribution to the time dependent deformation. Recently, for ufg-W with grain sizes of around 1 μm the same strain-rate dependent hardness difference was

measured as for sx-W. This led to the conclusion that the Peierls potential has the same influence in that microstructural state. Here, the grains are smaller, thus an additional contribution of grain boundaries, but also deformation governed by edge dislocations or impurity ratios, might be taken into account, which could cause the reduced hardness differences in the presently studied Cr [25].

With increasing T, a decreasing SRS is found for sx-Cr, since the influence of the thermally activated component slowly diminishes as expected (Fig. 3b). Compared to fcc-metals this conclusion seems reasonable; for fcc single crystals no SRS is found, as the thermally activated component is negligible at RT and below. For the ufg-Cr, the SRS remains constant underneath T_c, but significantly increases above T_c. While at RT the thermally activated component was represented by both, Peierls stress and grain boundary contributions, with increasing homologous testing temperature the contribution of the Peierls barriers slowly diminishes, as seen for sx-Cr. Concurrently, the grain boundary–dislocation interactions gain increased importance for the overall deformation behavior. Starting with an interaction of both thermally activated components (majorly depending on the microstructure) below T_c, the dislocation–grain boundary interactions become dominant once overcoming T_c. This idea also agrees well with the known deformation concepts and mechanisms in nc- and ufg fcc metals, where the SRS is dominantly caused by thermally activated dislocation motion, recombination, or relaxation at grain boundaries, and gets more pronounced at elevated temperatures, unless recrystallization of the microstructure occurs [26–28].

In this work, we studied the influence of microstructure, strain-rate, and temperature on the deformation behavior of Cr. The deformation behavior of sx-Cr is significantly affected by the testing temperature. Below a critical temperature T_c, the deformation is dominated by the movement of screw dislocations and thereby a kink-pair interaction. This leads to a high SRS at low homologous T, such as room temperature, which diminishes linearly with increasing T. Overcoming T_c, the thermally activated part is completely negligible and the deformation behavior of the bcc-metal has reached the characteristics of an fcc-metal. However, for the ufg-state our results lead to another conclusion. At room temperature a low SRS is determined, significantly reduced compared to the sx-state. This is explained by the higher athermal stress component, which leads to higher hardness and influences the evaluation of the m-value. Moreover, the refined microstructure itself might influence the deformation as well. Increasing T overcoming T_c, the thermally activated component increases and a higher SRS is measured. This is explained by thermally activated dislocation–grain boundary interactions in the ufg-state and can be rationalized in close relationship to the behavior of fcc ufg-materials. Overall, the described concepts presented are further applicable to all other bcc-materials and influence the thermally activated processes such as the brittle to ductile transition. However the absolute values and transition temperatures are thereby directly dependent on the respective critical temperature of each bcc-metal.

The authors acknowledge funding by Zukunftsfond Steiermark within project P6019 (V.M. & D.K.), the funding by FWF project "P-25325" (D.K.), and by the European Research Council under grant number: 340185 (V.M. & R.P.). Assistance by Dr. W. Heinz during high temperature experiments is acknowledged.

Supplementary data associated with this article can be found, in the online version, at http://dx.doi.org/10.1016/j.scriptamat.2015.05.001.

[1] A.S. Schneider, D. Kaufmann, B.G. Clark, C.P. Frick, P.A. Gruber, R. Mönig, O. Kraft, E. Arzt, Phys. Rev. Lett. 103 (2009) 105501.
[2] J.R. Greer, J.T.H. De Hosson, Prog. Mater. Sci. 56 (2011) 654.
[3] Q. Wei, S. Cheng, K.T. Ramesh, E. Ma, Mater. Sci. Eng. A 381 (2004) 77.
[4] Q. Wei, J. Mater. Sci. 42 (2007) 1709.
[5] J. May, H.W. Höppel, M. Göken, Mater. Sci. Forum 503–504 (2006) 781.
[6] H.W. Höppel, J. May, P. Eisenlohr, M. Göken, Int. J. Mater. Res. 96 (2005) 566.
[7] R. Gröger, V. Vitek, Int. J. Mater. Res. 100 (2009) 315.
[8] A. Seeger, Z. Metalkunde 72 (1981) 369.
[9] V. Maier, C. Schunk, M. Göken, K. Durst, Philos. Mag. (2015), http://dx.doi.org/10.1080/14786435.2014.982741.
[10] L.W. Meyer, M. Hockauf, A. Hohenwarter, S. Schneider, Mater. Sci. Forum 584–586 (2008) 405.
[11] A.S. Schneider, C.P. Frick, E. Arzt, W.J. Clegg, S. Korte, Philos. Mag. 93 (2013) 331.
[12] V. Maier, K. Durst, J. Mueller, B. Backes, H.W. Höppel, M. Göken, J. Mater. Res. 26 (2011) 1421.
[13] E. Lucon, E.v. Walle, M. Decreton, Fusion Eng. Des. 58-59 (2001) 767.
[14] U. Holzwarth, H. Stamm, J. Nucl. Mater. 300 (2002) 161.
[15] R. Wadsack, R. Pippan, B. Schedler, J. Nucl. Mater. 307–311 (2002) 701.
[16] Y. Harada, M. Ohmori, J. Mater. Proc. Technol. 153–154 (2004) 93.
[17] R. Wadsack, R. Pippan, B. Schedler, Fusion Eng. Des. 66–68 (2003) 265.
[18] W.C. Oliver, G.M. Pharr, J. Mater. Res. 7 (1992) 1564.
[19] D. Wu, J. Zhang, J.C. Huang, H. Bei, T.G. Nieh, Scr. Mater. 68 (2013) 118.
[20] S. Lee, Z. Horita, Mater. Trans. 53 (2012) 38.
[21] V. Provenzano, R. Valiev, D.G. Rickerby, G. Valdre, Nanostruct. Mater. 12 (1999) 1103.
[22] G. Simmons, H. Wang, Single crystal elastic constants and calculated aggregate properties - a Handbook, MIT Press, 1971.
[23] G.M. Cheng, W.Z. Xu, W.W. Jian, H. Yuan, M.H. Tsai, Y.T. Zhu, Y.F. Zhang, P.C. Millett, J. Mater. Res. 28 (2013) 1820.
[24] G.M. Cheng, W.W. Jian, W.Z. Xu, H. Yuan, P.C. Millett, Y.T. Zhu, Mater. Res. Lett. 1 (2013) 26.
[25] R. Gröger, V. Vitek, Acta Mater. 56 (2008) 5426.
[26] J. Bach, J.P. Liebig, H.W. Höppel, W. Blum, Philos. Mag. 93 (2013) 4331.
[27] M. Dao, L. Lu, R.J. Asaro, J.T.M. De Hosson, E. Ma, Acta Mater. 55 (2007) 4041.
[28] K. Durst, V. Maier, Cur. Opi. Solid State Mater. Sci. (2015), http://dx.doi.org/10.1016/j.cossms.2015.02.001.